

Study of the Mass-Ratio Distribution of Spectroscopic Binaries. II. The Boundaries of the Brown-Dwarf Desert as Seen with the APOGEE Spectroscopic Binaries

S. Shahaf^{*} and T. Mazeh

School of Physics and Astronomy, Tel Aviv University, Tel Aviv 69978, Israel

Accepted XXX. Received YYY; in original form ZZZ

ABSTRACT

Analysis of APOGEE DR12 stellar radial-velocities by Troup et al. (2016) affirmed the existence of the well-known Brown-Dwarf Desert (BDD). They detected a dearth of spectroscopic binaries (SB) with periods shorter than ~ 10 –30 days and secondaries with masses in the range of ~ 0.01 – $0.1 M_{\odot}$. We reconsider here their sample of binaries, focusing on 116 systems on the main sequence of the *Gaia* color-magnitude diagram, with mostly K-dwarf primaries. Using our recently devised algorithm to analyze the mass-ratio distribution of a sample of SBs we confirm the BDD existence and delineate its boundaries. For the K-dwarf APOGEE 1–25 days binaries, the companion-mass range of the BDD is ~ 0.02 – $0.2 M_{\odot}$. The mass ratio distribution of the long-period (25–500 days) binaries does not show any dearth at the q -range studied. Instead, their distribution displays a linear increase in $\log q$, implying a tendency towards low- q values. The limits of the BDD do not coincide with the frequently used mass limits of the brown-dwarf population, sometimes defined as 0.013 and $0.08 M_{\odot}$, based on theoretically derived stellar minimum masses for burning deuterium and hydrogen in their cores. Trying to draw the boundaries of the desert, we suggest either a wedged or trapezoidal shape. We discuss briefly different scenarios that can account for the formation of the BDD, in terms of differentiating between stellar secondaries and planets in particular, and compare this desert to the Neptunian desert that can distinguish between Jovian planets and super Earths of short periods.

Key words: binaries: spectroscopic – methods: statistical – methods: data analysis

1 INTRODUCTION

Large surveys of stellar radial-velocities (RV), performed in the quest for exo-planets (e.g., Queloz et al. 2000; Marcy & Butler 2000; Pepe et al. 2004; Bouchy et al. 2009), have discovered in the last few decades many spectroscopic binaries (SB) with large range of secondary masses. A few studies noticed a dearth of companions with ~ 0.01 – $0.1 M_{\odot}$ mass for systems with orbital periods shorter than ~ 100 days (e.g., Marcy & Butler 2000; Grether & Lineweaver 2006). Ma & Ge (2014) assembled a literature-collected catalogue of 64 low-mass secondaries, of 10–80 Jupiter masses ($M_{\text{JUP}} \sim 10^{-3} M_{\odot}$), hosted by FGK-type primaries. Their derived mass-period distribution suggested that at orbital periods shorter than 100 days, secondaries with masses of 35–55 M_{JUP} are nearly depleted. The observed dearth was named the Brown-Dwarf Desert (BDD), after the dim objects below $\sim 0.08 M_{\odot}$, which cannot ignite hydrogen burning in their

cores (e.g., Kumar 1962, 1963; Hayashi & Nakano 1963). In this view, the few detected brown-dwarf (BD) *secondaries* with short orbital periods (e.g., Bouchy et al. 2011; Triaud et al. 2017; Grieves et al. 2017; dos Santos et al. 2017; Beatty et al. 2018; Hodžić et al. 2018) are just oases found inside the ‘desert’.

The BDD probably enables us to *statistically* distinguish between the populations of small stellar companions and massive planets. The very existence of the BDD might even indicate two different mechanisms of formation, below (planets) and above (stellar secondaries) the BDD (e.g., Grether & Lineweaver 2006).

The observational characteristics of the BDD can shed some light on its origin (e.g., Marks et al. 2017). The shape and location of the desert in the period-secondary mass parameter space (e.g., Schlaufman 2018), and their dependence on the stellar mass and metallicity (e.g., Bouchy et al. 2011; Borgniet et al. 2017; Murphy et al. 2018), are of particular interest. For example, it is hard to imagine that the BDD abruptly disappears for periods longer than some limiting

* E-mail: sahar@wise.tau.ac.il

period, as presented by some studies. Instead, we can expect a transition region at which the gap between the stellar secondaries and the massive planets gradually closes.

To further study the BDD and its borders, one needs an unbiased sample of SB systems obtained by a well-defined large survey with high enough precision, so observational effects can be estimated and corrected for. A large sample is not enough, since the unknown inclination of each binary does not allow deriving the secondary mass, even in cases where the primary mass can be estimated. As it is well known, assignment of some expected value of the inclination to all systems can distort the resulting mass-ratio distribution (e.g., Mazeh & Goldberg 1992; Heacox 1995), and therefore in our case can twist the BDD boundaries.

To overcome this problem one needs to apply statistical tools that utilize the assumed spherical symmetry of the binary inclinations (e.g., Mazeh et al. 1992; Boffin et al. 1993; Curé et al. 2015; Van der Swaelmen et al. 2017). One of these tools is the modified mass function of single-lined spectroscopic binaries (SB1s), suggested recently by Shahaf et al. (2017). They showed that this parameter, when derived for a sample of SB1s, follows the underlying mass-ratio distribution.

A sample of SB1s that enabled the study of the BDD is the one recently released by APOGEE¹—the Apache Point Observatory Galactic Evolution Experiment (Majewski et al. 2017). APOGEE is an infrared spectroscopic survey of Milky Way stars, with obtained spectra that cover the H-band wavelengths, from 1.51 to 1.69 μm , with a resolving power of 22,500. The database contains spectra of over 146,000 stars, most of which were measured at several epochs. The binary sample became available with the thorough and careful analysis of Troup et al. (2016, T16 henceforth).

RVs were derived for most APOGEE spectra with a typical precision of ~ 100 m/s (Nidever et al. 2015). This precision enables the detection of stellar, sub-stellar and even giant planetary companions (e.g., Price-Whelan et al. 2018; Badenes et al. 2018; El-Badry et al. 2018). T16 performed an extensive study of APOGEE DR12, and focused on single-lined systems with at least 8 epochs taken during a period of ~ 3 years.

Their analysis yielded a “gold sample” of 382 SB1s, out of which 155 have been identified as having main-sequence (MS) primaries. T16 used their sample, considering binaries with MS and evolved primaries alike, to notice that the BDD extends up to only orbital separations of 0.1–0.2 AU, i.e., orbital periods of 10–30 days.

This work targets the BDD as manifested among the APOGEE systems with K-dwarf primaries, with the goal of delineating the BDD borders. In Section 2 we take advantage of the release of *Gaia* DR2 parallaxes and colors to validate the classification of the primaries of the sample, and focus of a subsample of 116 binaries with definite mass range, 0.5– $1M_{\odot}$. Although left with a relatively small sample, we try in Section 3 to draw the shape and location of the BDD in the period–secondary-mass parameter plane. This is done by applying the Shahaf et al. (2017) algorithm to derive the mass-ratio distribution of the sample in two period bins, in

order to determine the mass limits of the BDD, and by drawing either a wedged or trapezoidal shape for the boundaries of the desert. Section 4 shortly discusses the meaning of the BDD in terms of planetary and binary formation.

2 THE RESTRICTED APOGEE K-DWARF SAMPLE OF SPECTROSCOPIC BINARIES

Figure 1 displays a *Gaia* color-magnitude diagram (CMD, see Lindegren et al. 2018) of 150 binaries classified by T16 as having MS primaries, for which their parallaxes have been released by *Gaia* DR2. The gray-scale density map in the background represents the *Hipparcos* stars (Lindegren et al. 1997) measured by *Gaia*, used as a proxy for the expected CMD in the solar neighborhood. The MS and the giant branch are clearly separated in the diagram.

Figure 1 suggests that a few of T16 MS stars are actually giants or subgiants. Those were removed from the sample we analyzed. Additionally, in order to have a small range of primary masses we limited the sample to include only systems redder than *Gaia*’s BP–RP 1.0 mag, and required T16 mass estimates to be of 0.5– $1M_{\odot}$. These requirements resulted in a subsample of 117 targets.

One system, 2M13431527+1910491, had an orbit of ~ 87 days, with a minimum mass ratio (see below) larger than unity. This system required further study, careful error estimation of the orbital parameters in particular, and therefore was excluded from the sample of this study. Its location on the *Gaia* CMD is marked by a cyan pentagram. We are left with 116 stars that we define as the restricted sample, representing the K-dwarf SB1s detected by APOGEE.

For completeness we added to Figure 1 the double-lined spectroscopic systems (SB2) found in APOGEE spectra by El-Badry et al. (2018). Out of 64 SB2s with reported orbits, 51 were found in a cross-match with *Gaia*, and 18 were located on the CMD near the SB1 restricted K-star sample. As expected, most of these SB2s are located slightly above the MS of the CMD.

A histogram of the primary masses, as reported by T16, of our restricted sample of SB1s, is shown in Figure 2.

3 THE BROWN-DWARF DESERT AND ITS BOUNDARIES

For each of the 116 binaries of the restricted sample, we use its primary mass, m_1 , and the mass function, $f(m_1)$, reported by Troup et al. (2016), to calculate the reduced mass function, y , which can be expressed as:

$$y \equiv \frac{f(m_1)}{m_1} = \frac{q^3}{(1+q)^2} \sin^3 i, \quad (1)$$

where q is the mass ratio and i is the orbital inclination angle.

Since the reduced mass function, y , is a combination of two unknowns, q and i , one cannot directly infer the mass ratio of each system. However, as is well known, each value of y defines a minimal possible mass ratio, \mathcal{Q}_y , that can be determined by setting the inclination angle i in equation (1) to be 90° .

To facilitate the derivation of the mass-ratio distribution Shahaf et al. (2017) introduced a new observable, S ,

¹ APOGEE: <http://www.sdss3.org/surveys/apogee.php>

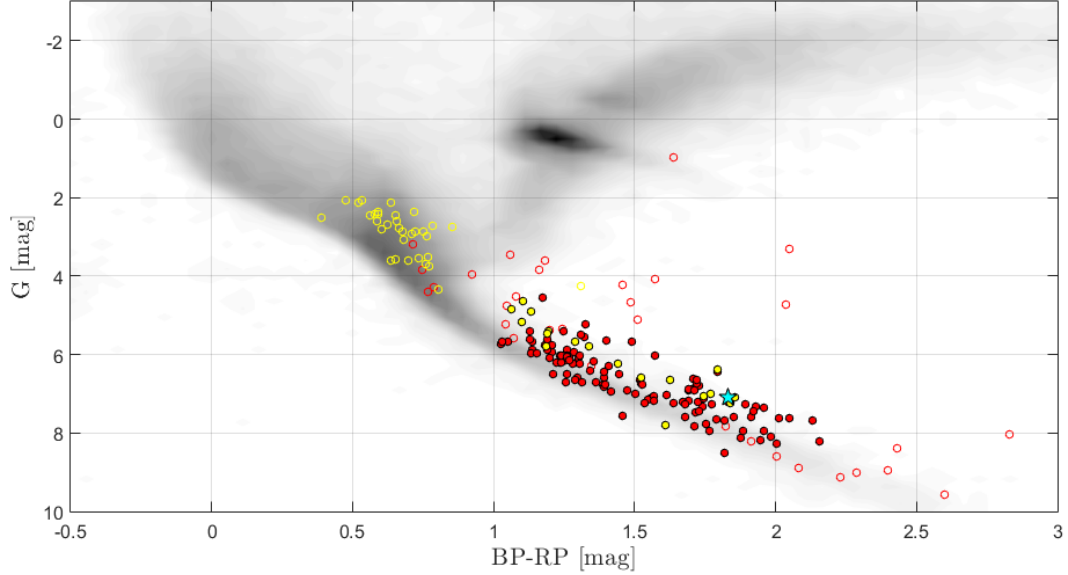


Figure 1. Restricted APOGEE SB1 sample (filled red circles) on *Gaia* CMD, overlaid on a gray-scale density map of *Hipparcos* stars, used as a proxy for the expected CMD in the solar neighborhood. Empty red circles represent SB1s that were rejected from the analyzed sample in this work, due to their CMD position or mass estimates provided by Troup et al. (2016). For completeness, 18 SB2s found by El-Badry et al. (2018) are presented as yellow circles. Empty yellow circles represent SB2s that are not in the color-magnitude range of the restricted sample. A cyan pentagram marks the location of 2M13431527+1910491, a binary with minimal mass-ratio larger than 1 that was excluded from the restricted APOGEE K-dwarf sample.

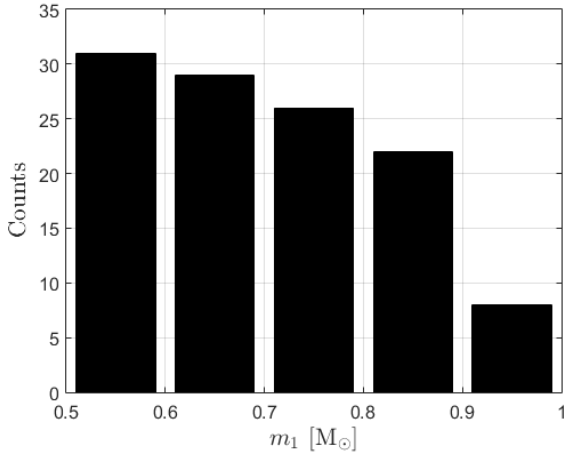


Figure 2. Primary-mass histogram of the restricted sample of 116 K-type MS primaries.

coined the ‘*modified* mass function’, and showed that the derived S distribution is similar to the underlying mass-ratio distribution of the sample. We therefore derived S for each target in the restricted sample,

$$S = 1 - \int_{\mathcal{Q}_y}^1 \sqrt{1 - y^{2/3} (1 + q)^{4/3} q^{-2}} dq, \quad (2)$$

and used its observed distribution as a proxy for the underlying mass ratio (see below).

Finally, we plot in Figure 3 the results on a period–

secondary-mass diagram, in order to obtain a clear view of the BDD. As a proxy for the secondary mass we use \bar{m}_2 ,

$$\bar{m}_2 \equiv 0.7 \cdot S M_{\odot}, \quad (3)$$

namely S multiplied by the typical primary mass value of the sample. For the 18 SB2 from El-Badry et al. (2018) we used the derived mass ratio instead of the modified mass functions. Kernel density estimation of the sample (see Botev et al. 2010) appears in gray-scale as a background.

3.1 The Mass-Ratio Distribution of the K-dwarf SB1s

We used the restricted sample to derive the mass-ratio distribution of two separate period bins, of 1–25 and 25–500 days, which resulted in sub-samples of 49 and 57 binaries, respectively. Each period bin was analyzed separately, by approximating the probability density function with a set of logarithmically equally-spaced boxcar functions. According to the Rice rule (Terrell & Scott 1985), and since the sample sizes are of ~ 50 binaries, we use eight bins that span $\log q$ from -2.4 to 0 , at spacing of 0.3 .

The mass-ratio distribution was then fitted by maximizing the likelihood of the sample, using an ensemble MCMC method (emcee, Foreman-Mackey et al. 2013). We assumed that the threshold for T16 APOGEE detection was an RV semi amplitude of 200 m/s, and corrected the induced observational bias accordingly (see Shahaf et al. 2017).

The resulting mass-ratio distributions are plotted in Figure 4. The fitted normalized distribution appears as a dashed gray line.

The thick black line represents the distribution cor-

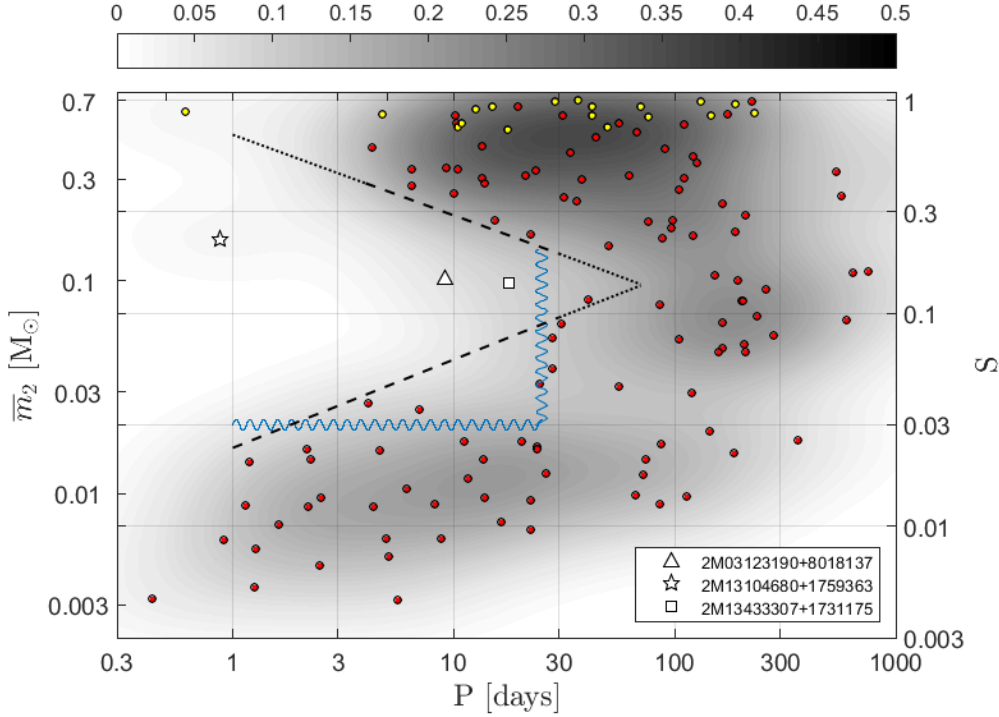


Figure 3. Estimated secondary mass, \bar{m}_2 , vs. binary period, P , plotted on a logarithmic scale. The horizontal axis on the right shows the value of the modified mass function, S . A kernel density estimate of the points appears in gray on the background. The restricted sample binaries are marked by red points, except three outliers that appear in white (see legend). Additionally, yellow points mark the 18 SB2s obtained from El-Badry et al. (2018), that were found to be located close to the restricted sample on the *Gaia* CMD. The figure suggests two alternative shapes of the desert borders (see text): a wedged-shape, with fitted slopes (dashed and dotted lines), and an eye-drawn trapezoid with blue serpentine line).

rected for systems undetected due to small RV amplitudes (see Shahaf et al. 2017). The magnitude of the correction is shown as a colored line below each figure.

The distribution derived in Figure 4 was based on the T16 SB1 sample only, ignoring the SB2s found by El-Badry et al. (2018). As all the SB2s had large mass ratio, close to unity, the resulting q -distribution was strongly biased at its high end. To correct for this effect we applied a 50% correction to the largest q bin. Still, this correction is highly arbitrary and therefore the values of last bin in each of the derived distributions are quite uncertain, and should not be used in any astrophysical discussion before further study.

The left panel, with the mass-ratio distribution of the short-period systems, clearly displays the BDD, extending over three bins at $-1.5 \lesssim \log q \lesssim -0.6$. In terms of the typical secondary mass, the desert is at

$$0.02 \lesssim m_2/M_\odot \lesssim 0.2. \quad (4)$$

The mass ratio distribution of the long-period (25–500 days) binaries does not display any dearth at the q -range studied. Instead, the resulting distribution suggests a linear increase in $\log q$, implying a tendency towards low- q values.

Figure 5 compares the modified mass function distribution (Shahaf et al. 2017) both with a mass-ratio distribution of a desert-shape and a linear distribution in $\log q$. The figure demonstrates the capacity of the modified mass function to follow the mass-ratio distribution in both cases. Note the small excess of the S distribution at the edge of the studied

range, which is inherent feature of the modified mass function (see equation 2). A code to derive the modified mass function is available on-line.²

3.2 The boundaries of the BDD

In this subsection we discuss two alternative ways to draw the boundaries of the BDD. Unfortunately, the SB1 sample is not large enough to differentiate between the two shapes. The two resulting shapes are similar, and the difference does not have an obvious impact on the discussion of the astrophysical implication of the desert.

3.2.1 Wedged-Shape Desert

Following Mazeh et al. (2016), we tried to delineate the low- and high-mass BDD borders by fitting the observed occurrence rate with a sigmoid function, relative to a linear borderline

$$\mathcal{M}_2 = a\mathcal{P} + b, \quad (5)$$

where \mathcal{M}_2 and \mathcal{P} represent $\log \frac{\bar{m}_2}{M_\odot}$ and $\log \frac{P}{\text{day}}$, respectively.

We modeled the probability for an observed system with

² <https://github.com/saharsh1/BinaryMassFunction>

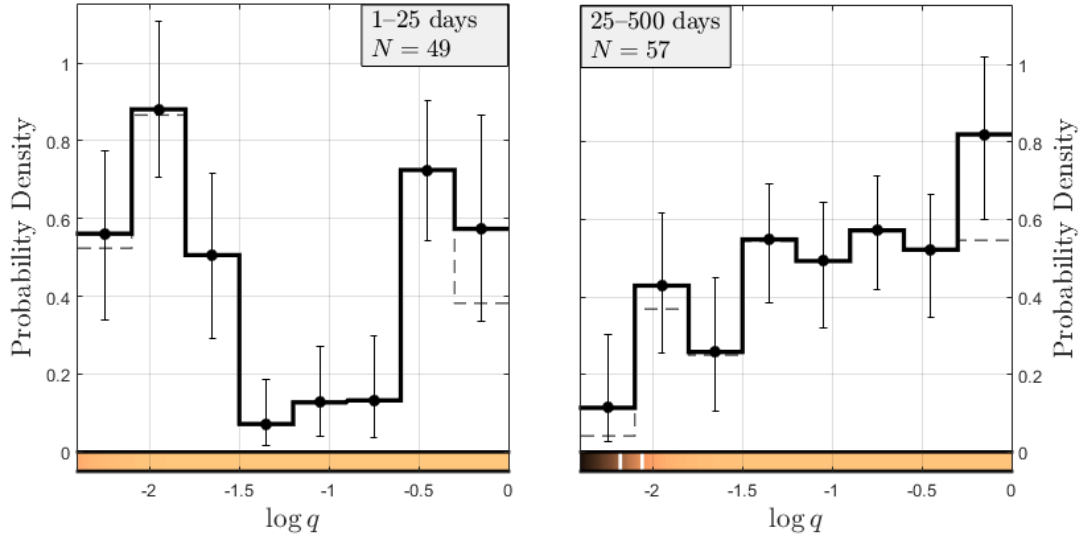


Figure 4. Derived mass-ratio distribution in two selected period bins. The thick black line represents the fitted box-car shaped model. The fitted bins are of constant width of 0.3 and span the range from -2.4 to 0 in $\log q$. The error bars represent 1σ confidence interval. The gray dashed line shows the fitted distribution before correcting for detection bias. The expected fraction of detected binaries as a function of $\log q$, given the assumed threshold of 200 m/s, appears as a bar below the fitted model, where black is no detection and copper is 100% detection. The two white lines on the bottom of the right panel represent the 50% and 75% percent detection probability. The sample presented on the left panel is of SB1s with shorter period range, and therefore its detection probability $\gtrsim 90\%$ throughout the fitted range.

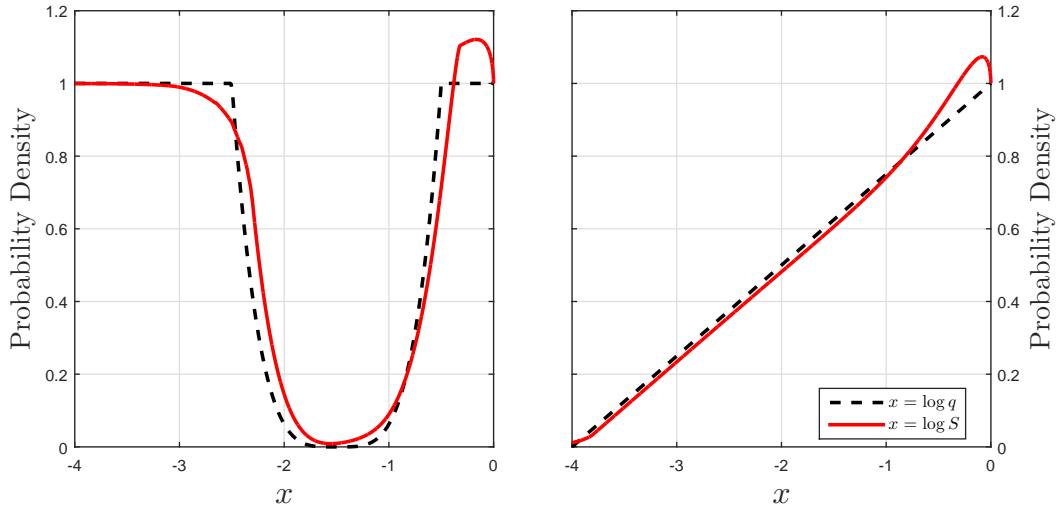


Figure 5. Desert-type (left) and linear in $\log q$ (right) mass-ratio distributions (black dashed) compared with the derived distribution of the modified mass function (red).

measured \mathcal{M}_2 and \mathcal{P} to be located at a distance d from the line as

$$\mathcal{F}(\mathcal{M}_2, \mathcal{P}; a, b) = A \left\{ \left[1 + e^{-d/\delta} \right]^{-1} + \Delta \right\}, \quad (6)$$

where δ is the transition-steepness, Δ the density inside the desert and A is a normalization factor. The distance d is taken as the distance of $(\mathcal{P}, \mathcal{M}_2)$ from the borderline, so that $d > 0$ outside the desert.

The parameters a , b , δ and Δ were estimated by max-

imizing the likelihood of the model for the location of the upper and lower borders, given the sample, using an MCMC ensemble sampler (see [Foreman-Mackey et al. 2013](#)).

The lower border was fitted with the 34 systems that have periods in the range of 1–30 days and $S < 0.1$. The upper border was fitted with the 15 systems that have periods in the range of 4–30 days and $S > 0.15$. The derived borders are represented in Figure 3 by a dashed line. The dotted

	a	b	δ	Δ
Upper	$-0.41^{+0.20}_{-0.25}$	$-0.28^{+0.26}_{-0.23}$	$0.005^{+0.013}_{-0.004}$	< 0.07
Lower	$0.40^{+0.12}_{-0.11}$	$-1.80^{+0.11}_{-0.09}$	$0.0025^{+0.0042}_{-0.0021}$	< 0.002

Table 1. Fitted borderline parameters. The fitted probability density inside the desert, Δ , was consistent with 0, therefore its 3σ upper limit is presented.

APOGEE ID	N	P [day]	K [km/s]	e
2M03123190	30	9.1756	8.10	0.414
+8018137		± 0.0033	± 0.12	± 0.011
2M13104680	9	0.878933	24.0	< 0.03
+1759363		± 0.000094	± 1.0	
2M13433307	13	17.76	6.31	0.549
+1731175		± 0.15	± 0.25	± 0.030

Table 2. Number of measurements, orbital period, RV semi amplitude and eccentricity of the three binaries located inside the proposed BDD borders.

line shows an extrapolation of the borders, such that the borderline covers the 1–70 day range.

3.2.2 Trapezoid-Shape Desert

As the lower boundary of the BDD is constrained by a small number of systems, we offer in Figure 3 alternative borderlines—horizontal and vertical straight lines. Their locations were chosen, somewhat arbitrarily at $S = 0.03$ and $P = 25$ days. The upper boundary is left as before. The trapezoid-shape limits are drawn with blue serpentine line.

3.3 Three Binaries inside the BDD

Figure 3 shows three binaries residing deep within the proposed BDD boundaries. Their fitted orbital parameters, as of all other “gold sample” binaries, were made available online by T16. For completeness we briefly summarize some of their properties in Table 2. To validate the results of T16, we re-fitted the orbital solution of the three systems and searched for center-of-mass acceleration, which may indicate a gravitational pull by a distant stellar companion. The table gives our P , K and e determination, all of which consistent with T16 (see below). We found that only the RVs of 2M13433307+1731175 displayed a possible acceleration of -0.053 ± 0.011 km/s/day.

The orbital solution of T16 for 2M13104680+1759363 displayed a large uncertainty, of over 800 km/s, on the RV semi-amplitude. Our analysis yielded an orbital solution consistent with that of T16 but with a substantial smaller uncertainty, given in Table 2. Since there were only 9 available RVs, we did not fit an acceleration component to this target.

4 DISCUSSION

We have presented here a detailed analysis of the BDD, based on a restricted sample of 116 APOGEE K-dwarf SB1s detected by T16. For binaries with ~ 1 –25 day period, the mass-ratio distribution reveals a dearth of secondaries with

mass of ~ 0.02 – $0.2M_{\odot}$. For binaries with longer periods (25–500 days) no desert is seen, and the derived mass-ratio distribution of the sample tends towards low- q values. The period limit of the BDD, ~ 25 days, corresponds to orbital separation of ~ 0.15 AU, as pointed out already by T16. In the \mathcal{P} - \mathcal{M}_2 plane, the desert is probably of a wedged or trapezoidal shape.

The mass limits of the BDD do not coincide with the generally accepted mass limits of the BD population, defined as 0.013 and $0.08M_{\odot}$, based on the minimum stellar mass required for deuterium and hydrogen burning in their cores, respectively (e.g., Burrows et al. 2001; Auddy et al. 2016), but see also Forbes & Loeb (2019). In particular, the findings are in contrast with the claim that the mass upper limit of the BDD coincides with the stellar/BD mass transition. This claim was difficult to explain, since it is not clear how the nuclear astrophysics of the stellar core can also surface in the binary formation of short-period systems.

One may think of two types of interpretation of the BDD:

(i) As an outcome of binary/planetary formation, the primordial density of binaries in the \mathcal{P} - \mathcal{M}_2 plane was flat, with no BDD. The desert was formed by some later mechanism that caused objects found in the BDD to ‘move away’ from the ‘restricted area’ (e.g., Armitage & Bonnell 2002; Damiani & Díaz 2016; Grunblatt et al. 2018; Vick et al. 2019). This could happen by

- Enlarging the mass of the companions found in the BDD, effectively pushing the systems up in the \mathcal{P} - \mathcal{M}_2 plane.
- Stripping part of the companions’ mass, effectively pushing systems down in the \mathcal{P} - \mathcal{M}_2 plane.
- Spiraling the secondaries into the primary, maybe by tidal interaction.
- Pushing the secondaries out towards larger orbits, maybe by tidal interaction.

(ii) The BDD is an outcome of a gap between two different formation mechanisms—binary formation with stellar-mass secondaries, and planetary formation with Jovian and smaller masses (e.g., Ma & Ge 2014; Chabrier et al. 2014). The binary formation has a lower mass limit larger than the upper mass limits of planets.

Note that if we accept the first class of interpretations, which assumes that the objects at the BDD were pushed out of the restricted area, we can naturally expect a wedged or trapezoidal shape. The effectiveness of the mechanism that clears up the BDD area, whatever its origin might be, could get weaker for longer periods and larger orbital separation. On the other hand, if we adopt the second interpretation, we still need to explain why the slope of the upper boundary, which is the lower envelop of the stellar secondaries, is clearly negative, whereas the slope of the lower boundary, which is the upper envelop of the planets, is definitely not negative.

The (almost) generally accepted paradigm is that planetary and binary formations operate with two different mechanisms. Binary formation is probably driven by fragmentation of the early contracting protostar (e.g., Bate & Bonnell 1997; Bonnell & Bate 2006; Bonnell et al. 2008; Riaz et al. 2018), whereas planets are formed by coagulation of small planetesimals in an accretion disc around the star (e.g., Pol-

lack et al. 1996; Goldreich et al. 2004; Levison et al. 2010). A natural consequence of the duality of the binary and planetary formations is the second interpretation of the BDD. Accordingly, the desert is the product of a lucky coincidence. For *short-period* orbits, the upper mass limit of planetary formation is smaller than the lower mass limit of stellar formation. This enables us to distinguish between the short-period planets and stellar secondaries.

Provided this is true, our analysis indicates that in the context of the BDD the distinction between a BD and a planet at $13M_{\text{Jup}}$, based on nuclear ignition of deuterium, is not very useful. We have shown that for the APOGEE K-dwarf sample, the BDD extends down only to about $\sim 20M_{\text{Jup}}$. In any case, ‘planet’ should be an attribute associated with a small-mass object orbiting a star, while a BD is termed to describe an object that fails to ignite hydrogen in its core, regardless of its dynamical properties.

In the analysis presented above three binaries clearly stand out in the middle of the desert. Their isolated locations deserve a special attention, based on the assumed mechanism behind the BDD. Were those systems pushed into the desert after their formation, maybe by some interaction with a third star through the Kozai-Lidov mechanism? This idea was suggested by Fabrycky & Tremaine (2007) to account for the formation of *all* short-period binaries (see also Mazeh & Shaham 1979). If so, we should find some evidence for those oases to have third distant faint companions, as in the case of HD 41004 Bb (see Zucker et al. 2003).

Alternatively, we should find that the frequency of binaries inside the BDD with third companions is higher than it is for systems outside the desert. Very recent study of Fontanive et al. (2019) suggests that this is the case for close giant planets, not necessarily inside the BDD. Currently, there are ~ 120 known planets that orbit a star that has a distant stellar companion, listed in a catalogue³ by Schwarz et al. (2016), but a careful analysis of the frequency of such systems is still not available.

Conversely, the desert might be not so dry at the first place (see Carmichael et al. 2019, and references therein). Some binaries could be formed at the middle of the BDD, because of some scarce initial conditions. We need more similar systems, followed by in-depth studies, to understand the nature of these special cases (e.g., WASP-128b, Hodžić et al. 2018).

The existence and characteristics of the BDD should be compared with the Neptunian desert found around G-dwarf primaries (e.g., Szabó & Kiss 2011; Mazeh et al. 2016), based mainly on the *Kepler* space-mission discoveries. The Neptunian desert also has a wedged shape at the \mathcal{P} - \mathcal{M}_2 plane, centered around $\sim 0.1M_{\text{Jup}}$, whereas the BDD of the K-dwarf APOGEE is *centered* around $\sim 70M_{\text{Jup}}$.

Similar to the possible role of the BDD, the Neptunian desert can distinguish between Jovian planets and super Earths of short periods. The formation of the desert is still debated (see, for example, Matsakos & Königl 2016; Ionov et al. 2018; Owen & Lai 2018, for theoretical discussion). The recent study of Szabó & Kálmán (2019) that considered the boundaries of the Neptunian desert and their dependence of the primary mass and temperature should shed some light

on its origin. Adopting the right interpretation, like in the BDD case, depends on the formation scenarios of the populations on the two sides of the desert.

Do the two deserts, separated by almost three orders of magnitude, send us similar messages, namely that they both were formed by mass limits of two different mechanisms? If so, then we are now facing three mechanisms of formation—stellar secondaries, Jovian *and* super-Earth planets. Again, in the short-period domain, the two deserts help us distinguish between the three populations, and should be used as clue for detailed modeling of their formation.

A critical test of this interpretation of each of the two deserts is the dependence of their location and shape on stellar and environment features, stellar mass and metallicity in particular (e.g., Bouchy et al. 2011; Guillot et al. 2014).

Large samples of short-period binaries will be available with the releases of the *Gaia* SB1 systems in the next few years.⁴ Large samples of transiting planets and BD secondaries around different types of primary stars are being discovered by TESS⁵ (Ricker et al. 2014), such as HD 202772A b (Wang et al. 2019) and HATS-71b (Bakos et al. 2018). The new findings will enable us to better understand the nature of both deserts in a few years.

ACKNOWLEDGEMENTS

We are indebted to the APOGEE team and to Troup and his group for the fantastic set of spectra and the careful analysis of the spectroscopic binaries. This study would not be possible without their seminal work. Special thanks to Simchon Faiglar for careful reading of the manuscript and enlightening comments. This research was supported by Grant No. 2016069 of the United States-Israel Binational Science Foundation (BSF) and by the Israeli Centers for Research Excellence (I-CORE, grant No. 1829/12).

REFERENCES

- Armitage P. J., Bonnell I. A., 2002, *MNRAS*, **330**, L11
Auddy S., Basu S., Valluri S. R., 2016, *Advances in Astronomy*, **2016**, 574327
Badenes C., et al., 2018, *ApJ*, **854**, 147
Bakos G. Á., et al., 2018, arXiv e-prints, p. arXiv:1812.09406
Bate M. R., Bonnell I. A., 1997, *MNRAS*, **285**, 33
Beatty T. G., Morley C. V., Curtis J. L., Burrows A., Davenport J. R. A., Montet B. T., 2018, *AJ*, **156**, 168
Boffin H. M. J., Cerf N., Paulus G., 1993, *A&A*, **271**, 125
Bonnell I. A., Bate M. R., 2006, *MNRAS*, **370**, 488
Bonnell I. A., Clark P., Bate M. R., 2008, *MNRAS*, **389**, 1556
Borgniet S., Lagrange A.-M., Meunier N., Galland F., 2017, *A&A*, **599**, A57
Botev Z. I., Grotowski J. F., Kroese D. P., 2010, arXiv e-prints, p. arXiv:1011.2602
Bouchy F., et al., 2009, *A&A*, **505**, 853
Bouchy F., et al., 2011, *A&A*, **533**, A83
Burrows A., Hubbard W. B., Lunine J. I., Liebert J., 2001, *Reviews of Modern Physics*, **73**, 719
Carmichael T., Latham D., Vanderburg A., 2019, arXiv e-prints,

³ <https://www.univie.ac.at/adg/schwarz/multiple.html>

⁴ <https://www.cosmos.esa.int/web/gaia/release>

⁵ TESS: <https://tess.gsfc.nasa.gov/>

- Chabrier G., Johansen A., Janson M., Rafikov R., 2014, in Beuther H., Klessen R. S., Dullemond C. P., Henning T., eds, *Protostars and Planets VI*. p. 619 ([arXiv:1401.7559](https://arxiv.org/abs/1401.7559)), [doi:10.2458/azu_uapress_9780816531240-ch027](https://doi.org/10.2458/azu_uapress_9780816531240-ch027)
- Curé M., Rial D. F., Cassetti J., Christen A., Boffin H. M. J., 2015, *A&A*, **573**, A86
- Damiani C., Díaz R. F., 2016, *A&A*, **589**, A55
- El-Badry K., et al., 2018, *MNRAS*, **476**, 528
- Fabrycky D., Tremaine S., 2007, *ApJ*, **669**, 1298
- Fontanive C., Rice K., Bonavita M., Lopez E., Mužić K., Biller B., 2019, *MNRAS*,
- Forbes J. C., Loeb A., 2019, *ApJ*, **871**, 227
- Foreman-Mackey D., et al., 2013, emcee: The MCMC Hammer, *Astrophysics Source Code Library* (ascl:1303.002)
- Goldreich P., Lithwick Y., Sari R., 2004, *ApJ*, **614**, 497
- Grether D., Lineweaver C. H., 2006, *ApJ*, **640**, 1051
- Grievés N., et al., 2017, *MNRAS*, **467**, 4264
- Grunblatt S. K., et al., 2018, *ApJ*, **861**, L5
- Guillot T., Lin D. N. C., Morel P., Havel M., Parmentier V., 2014, in *EAS Publications Series*. pp 327–336 ([arXiv:1409.7477](https://arxiv.org/abs/1409.7477)), [doi:10.1051/eas/1465009](https://doi.org/10.1051/eas/1465009)
- Hayashi C., Nakano T., 1963, *Progress of Theoretical Physics*, **30**, 460
- Heacox W. D., 1995, *AJ*, **109**, 2670
- Hodžić V., et al., 2018, *MNRAS*, **481**, 5091
- Ionov D. E., Pavlyuchenkov Y. N., Shematovich V. I., 2018, *MNRAS*, **476**, 5639
- Kumar S. S., 1962, *AJ*, **67**, 579
- Kumar S. S., 1963, *ApJ*, **137**, 1121
- Levison H. F., Thommes E., Duncan M. J., 2010, *AJ*, **139**, 1297
- Lindgren L., et al., 1997, *A&A*, **323**, L53
- Lindgren L., et al., 2018, *A&A*, **616**, A2
- Ma B., Ge J., 2014, *MNRAS*, **439**, 2781
- Majewski S. R., et al., 2017, *AJ*, **154**, 94
- Marcy G. W., Butler R. P., 2000, *PASP*, **112**, 137
- Marks M., et al., 2017, *A&A*, **605**, A11
- Matsakos T., Königl A., 2016, *ApJ*, **820**, L8
- Mazeh T., Goldberg D., 1992, *ApJ*, **394**, 592
- Mazeh T., Shaham J., 1979, *A&A*, **77**, 145
- Mazeh T., Goldberg D., Duquennoy A., Mayor M., 1992, *ApJ*, **401**, 265
- Mazeh T., Holczer T., Faigler S., 2016, *A&A*, **589**, A75
- Murphy S. J., Moe M., Kurtz D. W., Bedding T. R., Shibahashi H., Boffin H. M. J., 2018, *MNRAS*, **474**, 4322
- Nidever D. L., et al., 2015, *AJ*, **150**, 173
- Owen J. E., Lai D., 2018, *MNRAS*, **479**, 5012
- Pepe F., et al., 2004, *A&A*, **423**, 385
- Pollack J. B., Hubickyj O., Bodenheimer P., Lissauer J. J., Podolak M., Greenzweig Y., 1996, *Icarus*, **124**, 62
- Price-Whelan A. M., et al., 2018, *AJ*, **156**, 18
- Queloz D., et al., 2000, *A&A*, **354**, 99
- Riaz R., Vanaverbeke S., Schleicher D. R. G., 2018, *MNRAS*, **478**, 5460
- Ricker G. R., et al., 2014, *J. Astron. Telesc. Instruments, Syst.*, **9143**, 1
- Schlaufman K. C., 2018, *ApJ*, **853**, 37
- Schwarz R., Funk B., Zechner R., Bazsó Á., 2016, *MNRAS*, **460**, 3598
- Shahaf S., Mazeh T., Faigler S., 2017, *MNRAS*, **472**, 4497
- Szabó G. M., Kálmán S., 2019, arXiv e-prints,
- Szabó G. M., Kiss L. L., 2011, *The Astrophysical Journal*, **727**, L44
- Terrell G. R., Scott D. W., 1985, *Journal of the American Statistical Association*, **80**, 209
- Triaud A. H. M. J., et al., 2017, *MNRAS*, **467**, 1714
- Troup N. W., et al., 2016, *AJ*, **151**, 85
- Van der Swaelmen M., Boffin H. M. J., Jorissen A., Van Eck S., 2017, *A&A*, **597**, A68
- Vick M., Lai D., Anderson K. R., 2019, *MNRAS*, p. 356
- Wang S., et al., 2019, *AJ*, **157**, 51
- Zucker S., Mazeh T., Santos N. C., Udry S., Mayor M., 2003, *A&A*, **404**, 775
- dos Santos L. A., et al., 2017, *MNRAS*, **472**, 3425

This paper has been typeset from a $\text{\TeX}/\text{\LaTeX}$ file prepared by the author.